PERGAMON

International Journal of Solids and Structures 39 (2002) 1743–1756

INTERNATIONAL JOURNAL OF SOLIDS and STRUCTURES

www.elsevier.com/locate/ijsolstr

Transient response of an interface crack between dissimilar piezoelectric layers under mechanical impacts

Bin Gu, Shou-Wen Yu *, Xi-Qiao Feng *

Department of Engineering Mechanics, Tsinghua University, Beijing 100084, China

Received 27 August 2001; received in revised form 14 November 2001

Abstract

Using the integral transform and the Cauchy singular integral equation methods, the problem of an interface crack between two dissimilar piezoelectric layers under mechanical impacts is investigated under the permeable electrical boundary condition on the crack surface. The dynamic stress intensity factors (DSIFs) of both mode-I and II are determined. The effects of the crack configuration and the combinations of the constitutive parameters of the piezoelectric materials on the dynamic response are examined. The numerical calculation of the mode-I plane problem indicates that the DSIFs may be retarded or accelerated by specifying different combinations of material parameters. In addition, the parameters of the crack configuration, including the ratio of the crack length to the layer width and the ratio between the widths of two layers, exert a considerable influence on the DSIFs. The results seem useful for design of the piezoelectric structures and devices of high performance.

Keywords: Dynamic stress intensity factor; Interface crack; Piezoelectric material; Integral transform; Singular integral equation

1. Introduction

Piezoelectric materials possess intrinsic electromechanical coupling effects, by virtue of which they have found extensive applications in smart devices as electromechanical actuators and transducers. For example, they are used in active vibration and noise suppression of sensors in space structures, rockets, weapon systems, smart skin systems of submarines, and so on. The reliability of these structures depends on the knowledge of applied mechanical and electric disturbances. When cracks are present, they may grow under service load and affect the performance of structures. Due to the disadvantage of brittleness and low fracture toughness of piezoelectric materials, a considerable number of research works have been carried out to investigate the fracture behavior (see, e.g., Pak, 1990; Suo et al., 1992; Gao et al., 1997; Wang and Han, 1999; Qin, 2000; Qin and Zhang, 2000).

As viewed from application, on one hand, piezoelectric systems are liable to meet dynamic loads in service. On the other hand, some piezoelectric structures are usually designed to guide such signals as

* Corresponding authors. Tel./fax: +86-10-6277-2926.
E-mail address: yusw@mail.tsinghua.edu.cn (X.-Q. Feng).

0020-7683/02/$ - see front matter
PII: S0020-7683(02)00013-6

surface waves. In such cases, elastic waves are generated in a structure. In the presence of cracks, these waves are reflected and refracted, causing higher stress concentration than under the corresponding static loads. This may initiate an unstable crack growth and eventually the final failure of the structure. Consequently, dynamic fracture analysis of piezoelectric materials has received a considerable attention in the past decade. Li and Mataga (1996a,b) studied the dynamic crack propagation by means of the Wiener–Hopf and Cagniard–de Hoop techniques. They treated the crack boundaries as electrically conducting electrodes and a vacuum zone to meet Bleustein–Gulyaev waves. Using the integral transform techniques, Chen et al. (1998) solved the problem of an anti-plane Griffith crack moving along an interface of two dissimilar piezoelectric materials. Their results showed that the intensity factors of the anti-plane stresses and electric displacements depend on the moving speed of the crack and the material coefficients as well. Further, Chen and Yu (1997, 1998) investigated the anti-plane problems of a Griffith crack and a semi-infinite crack subjected to electromechanical impacts. It was found that the dynamic stress intensity factor (DSIF) depends not only on the mechanical impact, but on the electrical impact, the piezoelectric and dielectric coefficients also. In addition, their analysis showed that for anti-plane crack problems, the dynamic electric displacement intensity factor (DEDIF) always remains the same as the corresponding static value. Chen and Karihaloo (1999) deduced the solutions of a mode-III crack subjected to arbitrary electromechanical impacts. Narita and Shindo (1998) investigated the scattering of Love waves by a surface-breaking crack in a piezoelectric laminated medium by means of the path-integral technique. In addition, Shindo et al. (1996) presented a dynamic fracture analysis for a cracked electric medium under a uniform electric field. To date, nevertheless, analysis on dynamic in-plane problems is very limited. On the basis of the previous works, the transient response of a cracked strip subjected to plane electromechanical impacts was investigated by Wang and Yu (2000) making use of the integral transform and the singular integral equation methods. A great dependence of the DSIF and the dynamic energy release rate (DERR) on such parameters as the loading combination parameter and the ratio between the crack length and the strip width was illustrated. It was also found that in contrast with the mode-III crack as aforementioned, the DEDIF of a mode-I crack exhibited a considerable dynamic response.

As to crack face electrical boundary conditions, Suo et al. (1992) discussed several different assumptions in detail. Especially, they examined two limit cases of crack face electrical boundary conditions, namely the permeable condition and the insulating condition. More arguments about crack face electrical boundary conditions can be found in the literatures (see, e.g., Pak, 1990; Suo et al., 1992; Gao et al., 1997; Shindo et al., 1996). In this paper, the plane problem of an interface crack between two piezoelectric layers of finite widths under mechanical impacts is analyzed under the permeable electrical boundary condition, by means of the integral transform and the Cauchy singular integral equation methods. The dependence of the transient response on the crack configuration and the constitutive parameters of the dissimilar piezoelectric materials are discussed. For the special case of a homogeneous material, the results reduced from the present analysis are compared with those obtained by Wang and Yu (2000).

2. Formulation of the problem

Consider an interface crack of length $2c$ located between two piezoelectric layers in the form of an infinitely long strip subjected to mechanical impacts, as shown in Fig. 1. Refer to a Cartesian coordinate system (x, y, z) with the x-axis along the interface, and the z-axis normal to the interface and aligned with the poling axis. Assume that the piezoelectric ceramic strip is thick enough in the y-direction to allow for adopting the condition of plane strain. A complex impact load of tension and shearing is imposed on the crack surfaces.

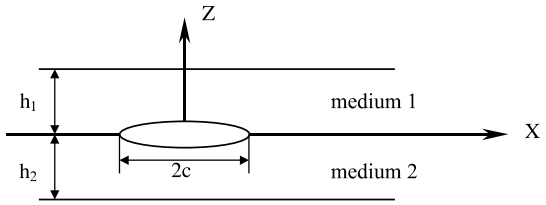

Fig. 1. Crack configuration.

Under the condition of plane strain, one has

$$\begin{aligned} &u_x = u(x,z,t), \qquad u_y = 0, \qquad u_z = w(x,z,t), \qquad \varepsilon_{yy} = 0, \\ &E_x = E_x(x,z,t), \qquad E_y = 0, \qquad E_z = E_z(x,z,t), \end{aligned} \tag{1}$$

where u_i and E_i denote the displacement and electric field vectors, respectively. Introducing the electric potential ϕ by $E_i = -\partial\phi/\partial x_i$, the linear constitutive relations of a transversely isotropic piezoelectric material are expressed as (Suo et al., 1992)

$$\begin{aligned} \sigma_{xx} &= c_{11}u_{,x} + c_{13}w_{,z} + e_{13}\phi_{,z}, \\ \sigma_{zz} &= c_{13}u_{,x} + c_{33}w_{,z} + e_{33}\phi_{,z}, \\ \sigma_{xz} &= c_{44}u_{,z} + c_{44}w_{,x} + e_{15}\phi_{,x}, \\ D_x &= e_{15}u_{,z} + e_{15}w_{,x} - \varepsilon_{11}\phi_{,x}, \\ D_z &= e_{13}u_{,x} + e_{33}w_{,z} - \varepsilon_{33}\phi_{,z}, \end{aligned} \tag{2}$$

where σ_{xx}, σ_{zz} and σ_{xz} are the stress components, D_x and D_z the electric displacement components, c_{11}, c_{13}, c_{33} and c_{44} the elastic moduli, e_{13}, e_{33} and e_{15} the piezoelectric coefficients, ε_{11} and ε_{33} the dielectric coefficients. The governing equations read

$$\begin{aligned} &c_{11}u_{,xx} + c_{44}u_{,zz} + (c_{13}+c_{44})w_{,xz} + (e_{13}+e_{15})\phi_{,xz} = \rho\frac{\partial^2 u}{\partial t^2}, \\ &(c_{13}+c_{44})u_{,xz} + c_{44}w_{,xx} + c_{33}w_{,zz} + e_{15}\phi_{,xx} + e_{33}\phi_{,zz} = \rho\frac{\partial^2 w}{\partial t^2}, \\ &(e_{13}+e_{15})u_{,xz} + e_{15}w_{,xx} + e_{33}w_{,zz} - \varepsilon_{11}\phi_{,xx} - \varepsilon_{33}\phi_{,zz} = 0, \end{aligned} \tag{3}$$

where ρ is the mass density.

The boundary conditions include the following three sets:

(i) *Crack surface conditions* ($|x| < c, z = 0$)

$$\begin{aligned} &\sigma_{xz}^{(1)}(x,0,t) = \sigma_{xz}^{(2)}(x,0,t) = -\tau_0 H(t), \\ &\sigma_{zz}^{(1)}(x,0,t) = \sigma_{zz}^{(2)}(x,0,t) = -\sigma_0 H(t), \\ &D_z^{(1)}(x,0,t) = D_z^{(2)}(x,0,t), \\ &\phi^{(1)}(x,0,t) = \phi^{(2)}(x,0,t). \end{aligned} \tag{4}$$

where the superscripts (1) and (2) denote media 1 and 2, respectively, τ_0 and σ_0 are the given amplitudes of the applied impact load, and $H(t)$ is the Heaviside function. Here the interface crack is assumed to be permeable (Suo et al., 1992).

(ii) *Continuity conditions on the interface* ($|x| > c, z = 0$)

$$\begin{aligned} &u^{(1)}(x,0,t) = u^{(2)}(x,0,t), \qquad w^{(1)}(x,0,t) = w^{(2)}(x,0,t),\\ &\phi^{(1)}(x,0,t) = \phi^{(2)}(x,0,t),\\ &\sigma_{xz}^{(1)}(x,0,t) = \sigma_{xz}^{(2)}(x,0,t), \qquad \sigma_{zz}^{(1)}(x,0,t) = \sigma_{zz}^{(2)}(x,0,t),\\ &D_z^{(1)}(x,0,t) = D_z^{(2)}(x,0,t). \end{aligned} \tag{5}$$

(iii) *Free boundary conditions* ($|x| > 0$)

$$\begin{aligned} &\sigma_{xz}^{(1)}(x,h_1,t) = \sigma_{zz}^{(1)}(x,h_1,t) = 0, \qquad D_z^{(1)}(x,h_1,t) = 0,\\ &\sigma_{xz}^{(2)}(x,-h_2,t) = \sigma_{zz}^{(2)}(x,-h_2,t) = 0, \qquad D_z^{(2)}(x,-h_2,t) = 0. \end{aligned} \tag{6}$$

3. Solution

Introducing the Laplace and Fourier transforms, the solutions of Eqs. (3) in the Laplace field, denoted by the superscript *, can be expressed as

$$\begin{aligned} u^{*(\alpha)}(x,z,p) &= \frac{1}{2\pi}\int_{-\infty}^{\infty}\left[\sum_{j=1}^{6} A_j^{(\alpha)}(s,p)\mathrm{e}^{\lambda_j^{(\alpha)}z}\right]\mathrm{e}^{-\mathrm{i}sx}\,\mathrm{d}s,\\ w^{*(\alpha)}(x,z,p) &= \frac{1}{2\pi}\int_{-\infty}^{\infty}\left[\sum_{j=1}^{6} a_j^{(\alpha)}(s,p)A_j^{(\alpha)}(s,p)\mathrm{e}^{\lambda_j^{(\alpha)}z}\right]\mathrm{e}^{-\mathrm{i}sx}\,\mathrm{d}s,\\ \phi^{*(\alpha)}(x,z,p) &= \frac{1}{2\pi}\int_{-\infty}^{\infty}\left[\sum_{j=1}^{6} b_j^{(\alpha)}(s,p)A_j^{(\alpha)}(s,p)\mathrm{e}^{\lambda_j^{(\alpha)}z}\right]\mathrm{e}^{-\mathrm{i}sx}\,\mathrm{d}s, \end{aligned} \tag{7}$$

where the superscript α ($\alpha = 1, 2$) stands for the corresponding medium. $a_j^{(\alpha)}(s,p)$, $b_j^{(\alpha)}(s,p)$ and $\lambda_j^{(\alpha)}(s,p)$ ($j = 1,\ldots,6$) are known functions of the Laplace variety p and the Fourier variety s (see Appendix A), and the parameters $A_j^{(\alpha)}(s,p)$ ($j = 1,\ldots,6$) are yet unknown.

Define the Laplace transformed dislocation density functions as (Wang and Yu, 2000)

$$\begin{aligned} f^*(x,p) &= \frac{\partial[u^{*(1)}(x,0,p) - u^{*(2)}(x,0,p)]}{\partial x},\\ g^*(x,p) &= \frac{\partial[w^{*(1)}(x,0,p) - w^{*(2)}(x,0,p)]}{\partial x}. \end{aligned} \tag{8}$$

Substituting Eqs. (7) into the constitutive equations (2) and then into the Laplace transformed boundary conditions in Eqs. (4)–(6) and using Eqs. (8), we obtain the following coupled singular integral equations:

$$\mathbf{A}\boldsymbol{\varphi}(x) + \frac{1}{\pi}\int_{-c}^{c}\mathbf{B}\frac{\boldsymbol{\varphi}(t)}{t-x}\,\mathrm{d}t + \frac{1}{\pi}\int_{-c}^{c}\mathbf{Q}(x,t)\boldsymbol{\varphi}(t)\,\mathrm{d}t = \mathbf{L}(x), \tag{9}$$

where $\mathbf{A}$ and $\mathbf{B}$ are two known constant matrixes with respect to the material constants in Eqs. (2), and $\mathbf{Q}(x,t)$ is a known function matrix (Appendix B). Throughout the paper, a boldface stands for a matrix or a vector. $\boldsymbol{\varphi}(t) = [f^*(t,p), g^*(t,p)]^{\mathrm{T}}$ is the dislocation density function vector to be solved, and $\mathbf{L}(x) = [-\tau_0/p, -\sigma_0/p]^{\mathrm{T}}$ is the known load vector. The single value condition is expressed as

$$\int_{-c}^{c}\boldsymbol{\varphi}(t)\,\mathrm{d}t = 0. \tag{10}$$

Using $x = cr$ and $t = cu$, Eq. (9) can be normalized in the form

$$\mathbf{A}\boldsymbol{\varphi}(r) + \frac{1}{\pi}\int_{-1}^{1}\mathbf{B}\frac{\boldsymbol{\varphi}(u)}{u-r}\,\mathrm{d}u + \frac{c}{\pi}\int_{-1}^{1}\mathbf{Q}(r,u)\boldsymbol{\varphi}(u)\,\mathrm{d}u = \mathbf{L}(r). \tag{11}$$

To solve the Cauchy singular integral equation (11) of the second type, an approximate method described in Shen and Kuang (1998) is employed. The regularization of Eq. (11) leads to

$$\boldsymbol{\psi}(r) + \frac{1}{\pi}\int_{-1}^{1}\frac{\boldsymbol{\psi}(u)}{u-r}\mathrm{d}u + \frac{c}{\pi}\int_{-1}^{1}\overline{\mathbf{Q}}(r,u)\boldsymbol{\psi}(u)\,\mathrm{d}u = \overline{\mathbf{L}}(r), \tag{12}$$

where

$$\boldsymbol{\psi}(u) = \mathbf{R}^{-1}\boldsymbol{\varphi}(u), \qquad \overline{\mathbf{Q}}(r,u) = \mathbf{R}^{-1}\mathbf{B}^{-1}\mathbf{Q}(r,u)\mathbf{R}, \qquad \overline{\mathbf{L}}(r) = \mathbf{R}^{-1}\mathbf{B}^{-1}\mathbf{L}(r), \tag{13}$$

$\boldsymbol{\Lambda}$ and $\mathbf{R}$ are the eigenvalue matrix and the eigenvector matrix of the determinant $(\mathbf{B}^{-1}\mathbf{A})$, respectively. They satisfy the following equality:

$$\mathbf{B}^{-1}\mathbf{A} = \mathbf{R}\boldsymbol{\Lambda}\mathbf{R}^{-1}. \tag{14}$$

The solutions of Eq. (12) can be expressed in the form

$$\boldsymbol{\psi}(x) = \begin{bmatrix} W_1(x) & 0 \\ 0 & W_2(x) \end{bmatrix}\begin{bmatrix} \sum_{k=0}^{\infty} A_k P_k^{(\alpha_1,\beta_1)}(x) \\ \sum_{k=0}^{\infty} B_k P_k^{(\alpha_2,\beta_2)}(x) \end{bmatrix}, \tag{15}$$

where $P_k^{(\alpha_j,\beta_j)}(x)$ $(j = 1, 2)$ are the Jacobi polynomials, and $W_j(x) = (1-x)^{\alpha_j}(1+x)^{\beta_j}$ is the weight function of Jacobi polynomials with

$$\alpha_j = -\frac{1}{2} + \frac{\mathrm{i}}{2\pi}\ln\frac{1-\mathrm{i}\gamma_j}{1+\mathrm{i}\gamma_j}, \qquad \beta_j = -\frac{1}{2} - \frac{\mathrm{i}}{2\pi}\ln\frac{1-\mathrm{i}\gamma_j}{1+\mathrm{i}\gamma_j}, \tag{16}$$

where γ_j are the elements of the eigenvalue matrix $\boldsymbol{\Lambda}$.

By considering the orthogonality relations of Jacobi polynomials

$$\int_{-1}^{1} W(x)P_k^{(\alpha,\beta)}(x)P_j^{(\alpha,\beta)}(x)\,\mathrm{d}x = \begin{cases} 0 & \text{when } k \neq j \\ \theta_k^{(\alpha,\beta)} = \frac{2^{(\alpha+\beta+1)}\Gamma(\alpha+k+1)\Gamma(\beta+k+1)}{k!(\alpha+\beta+2k+1)\Gamma(\alpha+\beta+k+1)} & \text{when } k = j \end{cases}, \tag{17}$$

in conjunction with $P_0^{(\alpha,\beta)}(x) = 1$, it can be concluded that the single value condition (10) is identically satisfied provided that $A_0 = B_0 = 0$.

Substituting Eq. (15) into (12) and using the following relation (Shen and Kuang, 1998)

$$\gamma W(r)P_k^{(\alpha,\beta)}(r) + \frac{1}{\pi}\int_{-1}^{1} W(u)P_k^{(\alpha,\beta)}(u)\frac{\mathrm{d}u}{u-r} = \begin{cases} \frac{(1+\gamma^2)^{1/2}}{2}P_{k-1}^{(-\alpha,-\beta)}(r) & (|r|<1), \\ \frac{(1+\gamma^2)^{1/2}}{2}\left[(r-1)^{\alpha}(r+1)^{\beta}P_k^{(\alpha,\beta)}(r) + G_k^{\infty}(r)\right] & (|r|>1), \end{cases} \tag{18}$$

where $G_k^{\infty}(r)$ is the principal part of $W_k(r)P_k^{(\alpha,\beta)}(r)$ at infinity, the singularity of Eq. (12) can be eliminated. Then using Eq. (17), the following algebraic equations are deduced

$$\begin{aligned} &\sum_{k=1}^{N}\left[T_{lk}^{11}A_k + T_{lk}^{12}B_k\right] = L_l^{\mathrm{e}1}, \\ &\sum_{k=1}^{N}\left[T_{lk}^{21}A_k + T_{lk}^{22}B_k\right] = L_l^{\mathrm{e}2}, \end{aligned} \tag{19}$$

where

$$T_{lk}^{ij} = \frac{(1+\gamma_i^2)^{1/2}}{2}\theta_{k-1}^{(-\alpha_i,-\beta_i)}\delta_{l(k-1)}\delta_{ij} + \frac{c}{\pi}\int_{-1}^{1}\int_{-1}^{1} W_{-i}(r)P_l^{(-\alpha_i,-\beta_i)}(r)\overline{q}_{ij}(u,r)W_j(u)P_k^{(\alpha_j,\beta_j)}(u)\,\mathrm{d}u\,\mathrm{d}r,$$
$$L_l^{ei} = \int_{-1}^{1} W_{-i}(r)P_l^{(-\alpha_i,-\beta_i)}(r)\overline{L}_i(r)\,\mathrm{d}r \quad (l=0,1,\ldots,N-1,\ \ i,j=1,2), \tag{20}$$

with $W_{-j}(x) = (1-x)^{-\alpha_j}(1+x)^{-\beta_j}$ and δ_{ij} being the Kronecker Delta function.

After the constants A_k and B_k $(k=1,2,\ldots,N)$ have been determined from Eqs. (19), define the equivalent DSIF as

$$\mathbf{K}^{e^*} = \begin{bmatrix} K_{\mathrm{II}}^{e^*} \\ K_{\mathrm{I}}^{e^*} \end{bmatrix} = \sqrt{2c}\lim_{r\to 1^+}\begin{bmatrix} (r-1)^{\alpha_1} & 0 \\ 0 & (r-1)^{\alpha_2} \end{bmatrix}\left[\mathbf{\Lambda\psi}(r) + \frac{1}{\pi}\int_{-1}^{1}\frac{\boldsymbol{\psi}(u)}{u-r}\,\mathrm{d}u + \frac{c}{\pi}\int_{-1}^{1}\overline{\mathbf{Q}}(r,u)\boldsymbol{\psi}(u)\,\mathrm{d}u\right]. \tag{21}$$

Then comparing the right-hand sides of Eqs. (11) and (12), one can obtain the relation between the actual DSIF and the equivalent DSIF as

$$\mathbf{K}^* = \mathbf{BRK}^{e^*}. \tag{22}$$

Finally, the DSIFs (mode-I and II) at the right crack tip in the Laplace field can be deduced as

$$\begin{bmatrix} K_{\mathrm{II}}^* \\ K_{\mathrm{I}}^* \end{bmatrix} = \sqrt{2c}\mathbf{BR}\sum_{k=1}^{N}\begin{bmatrix} \frac{-(1+\gamma_1^2)^{1/2}}{\sqrt{2}}2^{\beta_1}P_k^{(\alpha_1,\beta_1)}(1)A_k \\ \frac{-(1+\gamma_2^2)^{1/2}}{\sqrt{2}}2^{\beta_2}P_k^{(\alpha_2,\beta_2)}(1)B_k \end{bmatrix}. \tag{23}$$

Applying the inverse Laplace transforms by the method in Wang and Yu (2000), K_{I} and K_{II} in the time domain can be obtained.

4. Examples and discussion

It is noted that in the calculation of $q_{ij}(x,t)$ in (B.5), for most impact problems, there is no pole on the integral path along the x-axis, and therefore the integrals in these equations can be calculated directly. To illustrate the basic features of the solution, numerical calculations for cracked piezoelectric layers of PZT-5H have been carried out. To compare with the results in Wang and Yu (2000), we consider only the mode-I plane problem (i.e., $\tau_0 = 0$ and $\sigma_0 \neq 0$) and our attention is focused on the mode-I DSIF though it is coupled with the mode-II DSIF. For now, we assume $h_1 = h$. The following material parameters are used (Narita and Shindo, 1998):

$$\begin{aligned}
&c_{11}^{(1)} = 12.6\times10^{10}\ \mathrm{N/m^2}, \quad c_{11}^{(2)}/c_{11}^{(1)} = r_1, && c_{13}^{(1)} = 5.3\times10^{10}\ \mathrm{N/m^2}, \quad c_{13}^{(2)}/c_{13}^{(1)} = r_2,\\
&c_{33}^{(1)} = 11.7\times10^{10}\ \mathrm{N/m^2}, \quad c_{33}^{(2)}/c_{33}^{(1)} = r_3, && c_{44}^{(1)} = 3.53\times10^{10}\ \mathrm{N/m^2}, \quad c_{44}^{(2)}/c_{44}^{(1)} = r_4,\\
&e_{13}^{(1)} = -6.5\ \mathrm{C/m^2}, \quad e_{13}^{(2)}/e_{13}^{(1)} = r_5, && e_{33}^{(1)} = 23.3\ \mathrm{C/m^2}, \quad e_{33}^{(2)}/e_{33}^{(1)} = r_6,\\
&e_{15}^{(1)} = 17.0\ \mathrm{C/m^2}, \quad e_{15}^{(2)}/e_{15}^{(1)} = r_7, && \varepsilon_{11}^{(1)} = 151\times10^{-10}\ \mathrm{C/Vm}, \quad \varepsilon_{11}^{(2)}/\varepsilon_{11}^{(1)} = r_8,\\
&\varepsilon_{33}^{(1)} = 130\times10^{-10}\ \mathrm{C/Vm}, \quad \varepsilon_{33}^{(2)}/\varepsilon_{33}^{(1)} = r_9, && \rho^{(1)} = 7500\ \mathrm{Kg/m^3}, \quad \rho^{(2)}/\rho^{(1)} = r_{10}.
\end{aligned}$$

For comparison, the non-dimensional parameters $K_{\mathrm{I}}/K_{\mathrm{I0}}$ and $K_{\mathrm{II}}/K_{\mathrm{II0}}$ are introduced, where $K_{\mathrm{I0}} = K_{\mathrm{II0}} = \sigma_0\sqrt{c}$. Furthermore, the normalized time vt/c is used with $v = [(c_{33}^{(1)} + e_{33}^{(1)^2}/\varepsilon_{33}^{(1)})/\rho^{(1)}]^{1/2}$.

Our results are plotted in Figs. 2–14. It can be seen that the DSIFs under impact increase quickly, reach the maximal value and then drive to the corresponding static value. This can be understood by the impact effect of the incident elastic waves and the diffraction of the crack and the free boundary. As the results of

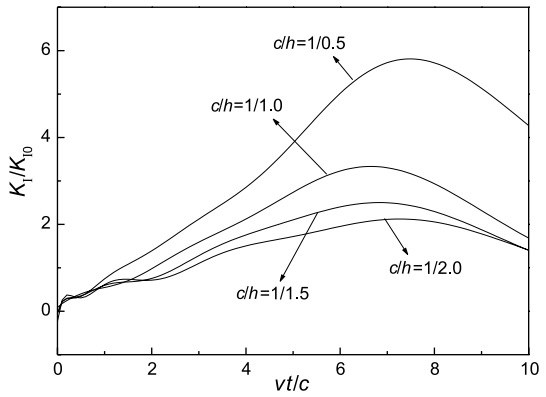

Fig. 2. Normalized mode-I DSIF versus normalized time for different values of c/h ($h_2/h = 1/1.0$, $r_1 = r_2 = 1.0$, $r_3 = 2.0$, $r_4 = \cdots = r_{10} = 1.0$).

their superposition, the DSIFs increase rapidly and approach to the static state when the wave diffraction drops off. It is also noted that the wave diffraction is related to the structural configuration and the material parameters. This will be illustrated in what follows.

Figs. 2–4 indicate the effects of the crack configuration, including the ratio of the crack length to the width of medium 1, c/h, and the ratio between the widths of the two layers, h_2/h, on the dynamic response. It is clearly shown from Figs. 2 and 3 that the larger the value of c/h, the higher is the maximal value of the DSIF, and the stronger is the oscillation of the dynamic response of either a homogeneous material or a laminated material. On the contrary, the larger the value of h_2/h, the lower is the DSIF (Fig. 4). Therefore, it can be concluded that the DSIF depends significantly on the free boundary.

The effects of material combinations can be seen from Figs. 5–14. It can be concluded from Figs. 5–8 that the different elastic moduli have different influence on the DSIF. The maximal value of the DSIF decreases with the increase in the value of r_1 (Fig. 5). The same phenomenon can also be found for the combination parameters r_2 (Fig. 6) and r_4 (Fig. 8). On the contrary, the maximal value of the DSIF increases as the value of r_3 increases (Fig. 7). As seen from the Figs. 9 and 10, the DSIF may be retarded by increasing the values of r_1, r_2, r_4, r_5 and r_6.

Comparing with the effects of the elastic moduli, however, the effects of the combination parameters of the piezoelectric coefficients are weaker distinctly. Furthermore, it is shown in Fig. 11 that the DSIF is

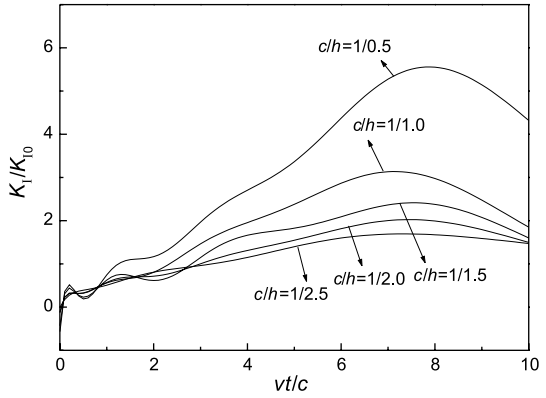

Fig. 3. Normalized mode-I DSIF versus normalized time for different values of c/h ($h_2/h = 1/1.0$, $r_1 = \cdots = r_{10} = 1.0$).

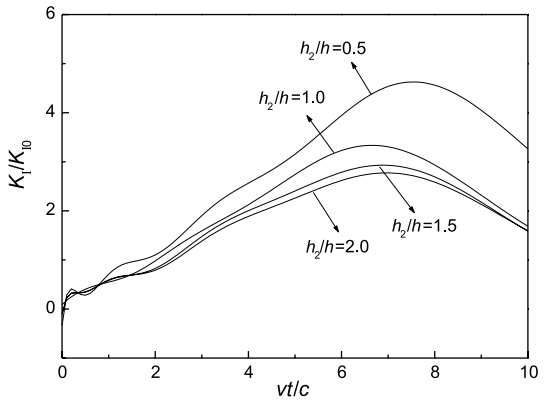

Fig. 4. Normalized mode-I DSIF versus normalized time for different values of h_2/h ($c/h = 1/1.0$, $r_1 = r_2 = 1.0$, $r_3 = 2.0$, $r_4 = \cdots = r_{10} = 1.0$).

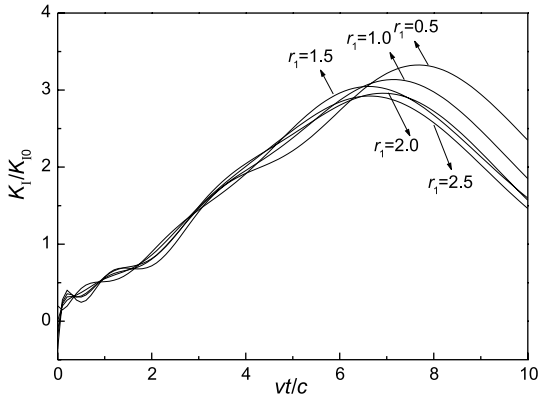

Fig. 5. Normalized mode-I DSIF versus normalized time for different values of r_1 ($c/h = 1/1.0$, $h_2/h = 1/1.0$, $r_2 = \cdots = r_{10} = 1.0$).

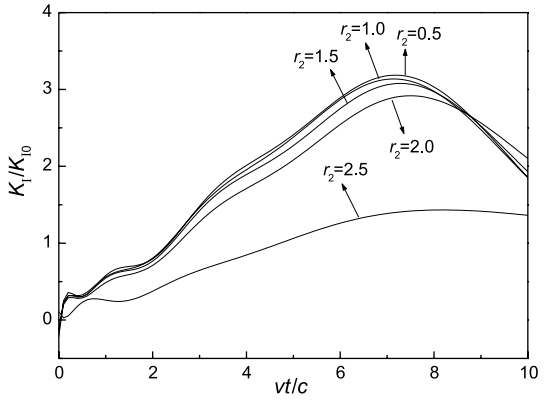

Fig. 6. Normalized mode-I DSIF versus normalized time for different values of r_2 ($c/h = 1/1.0$, $h_2/h = 1/1.0$, $r_1 = 1.0$, $r_3 = \cdots = r_{10} = 1.0$).

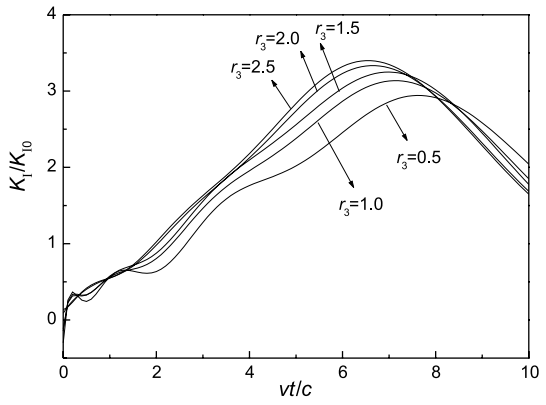

Fig. 7. Normalized mode-I DSIF versus normalized time for different values of r_3 ($c/h = 1/1.0$, $h_2/h = 1/1.0$, $r_1 = r_2 = 1.0$, $r_4 = \cdots = r_{10} = 1.0$).

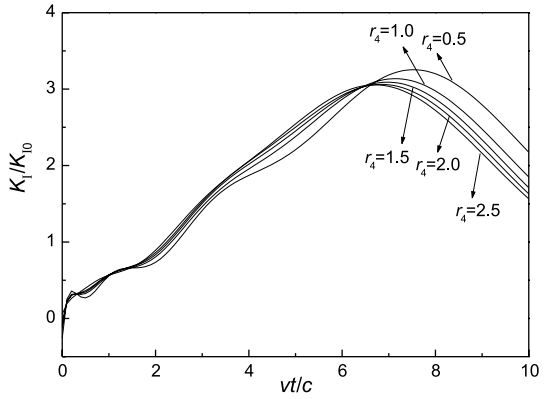

Fig. 8. Normalized mode-I DSIF versus normalized time for different values of r_4 ($c/h = 1/1.0$, $h_2/h = 1/1.0$, $r_1 = \cdots = r_3 = 1.0$, $r_5 = \cdots = r_{10} = 1.0$).

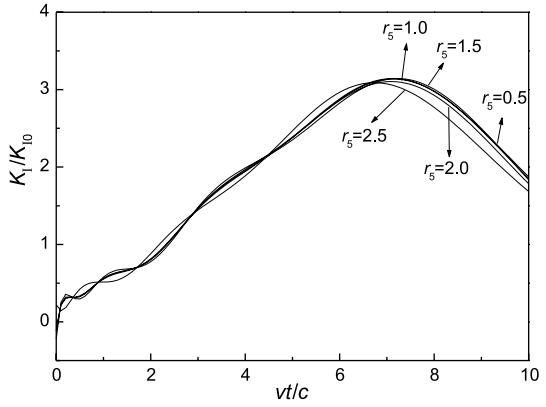

Fig. 9. Normalized mode-I DSIF versus normalized time for different values of r_5 ($c/h = 1/1.0$, $h_2/h = 1/1.0$, $r_1 = \cdots = r_4 = 1.0$, $r_6 = \cdots = r_{10} = 1.0$).

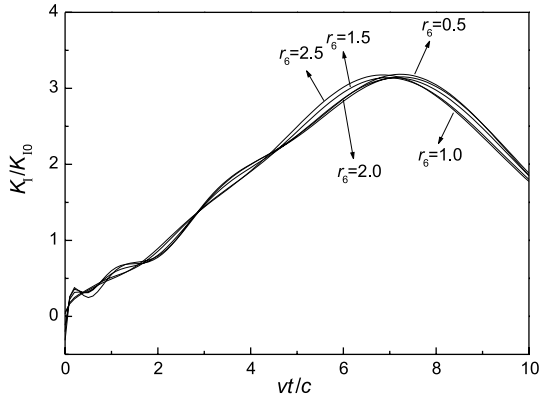

Fig. 10. Normalized mode-I DSIF versus normalized time for different values of r_6 ($c/h = 1/1.0$, $h_2/h = 1/1.0$, $r_1 = \cdots = r_5 = 1.0$, $r_7 = \cdots = r_{10} = 1.0$).

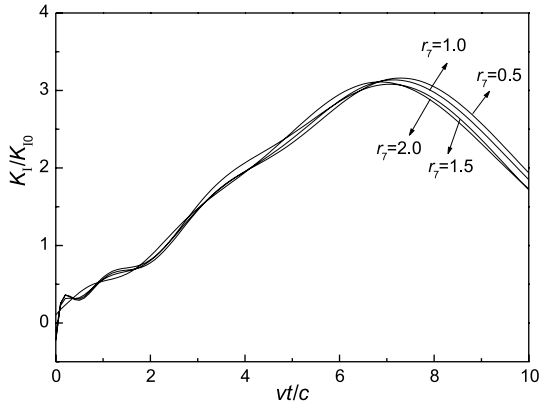

Fig. 11. Normalized mode-I DSIF versus normalized time for different values of r_7 ($c/h = 1/1.0$, $h_2/h = 1/1.0$, $r_1 = \cdots = r_6 = 1.0$, $r_8 = \cdots = r_{10} = 1.0$).

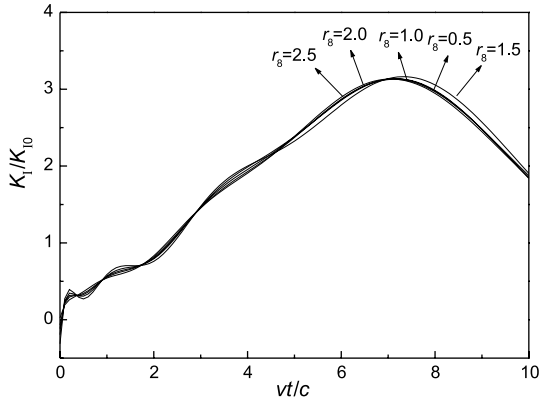

Fig. 12. Normalized mode-I DSIF versus normalized time for different values of r_8 ($c/h = 1/1.0$, $h_2/h = 1/1.0$, $r_1 = \cdots = r_7 = 1.0$, $r_9 = r_{10} = 1.0$).

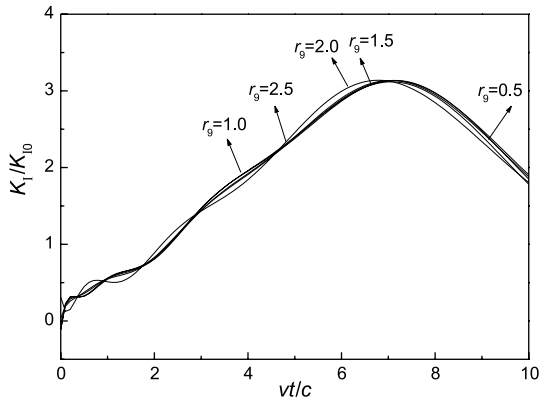

Fig. 13. Normalized mode-I DSIF versus normalized time for different values of r_9 ($c/h = 1/1.0$, $h_2/h = 1/1.0$, $r_1 = \cdots = r_8 = 1.0$, $r_{10} = 1.0$).

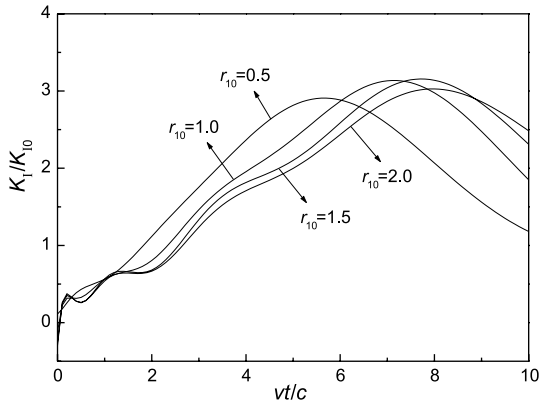

Fig. 14. Normalized mode-I DSIF versus normalized time for different values of r_{10} ($c/h = 1/1.0$, $h_2/h = 1/1.0$, $r_1 = \cdots = r_9 = 1.0$).

always promoted no matter that the value of r_7 increases or decreases from $r_7 = 1$, though the effect is not dramatic. This means that the DSIF has the lowest value in a homogeneous medium. The combinations of the dielectric constants, r_8 and r_9, have little influence on the DSIF, as shown in Figs. 12 and 13. The results in Fig. 14 indicate that the time when the DSIF reaches the peak value increases as r_{10} increases. Generally, a value of r_{10} lower than one leads to a lower peak value of the DSIF.

Comparing with the results of Wang and Yu (2000) for the case of a homogeneous material under the impermeable electrical boundary conditions, the present paper emphasizes the effects of the material combinations, which are of engineering significance.

5. Conclusions

The transient response of a Griffith crack between dissimilar piezoelectric layers subjected to mechanical impacts under the permeable electrical boundary condition on crack surfaces is investigated by using the integral transform and the Cauchy singular integral equation methods.

It is found from the numerical calculation that the ratio of the crack length to the layer width, c/h, has a significant influence on the DSIF. With the increase in c/h, the maximal value of the DSIF increases and the oscillation of the dynamic response becomes stronger. On the other hand, the maximal value of the DSIF decreases with the increase in h_2/h. Our analysis also shows that the dynamic response of an interface crack depends to different extents on the combinations of different constitutive parameters of the piezoelectric laminate. For a specific material (say medium 1 in the paper), increasing the ratios of some parameters of the two materials (e.g., r_1, r_6) may inhibit the DSIF, while an increase in the ratios of some other parameters (e.g., r_3) may promote the DSIF. The dielectric constants of the two materials have little influence on the DSIF.

The analysis on the effects of the crack configuration and the material parameters on the dynamic response of a cracked piezoelectric laminate leads to the conclusion that to enhance the performance and reliability of piezoelectric structures and devices, the materials should be chosen appropriately with a combination of constitutive parameters to yield a low DSIF under impacts. The method presented in this paper provides a tool for such a choice. Though the present work is centered on a permeable interface crack between two piezoelectric layers subjected to mechanical loading, this analysis method can be extended easily to other cases, e.g., electric loading or the insulating boundary condition on crack surfaces.

Acknowledgements

This project is supported by the National Natural Science Foundation of China (grant no. 19891180), the Education Ministry of China and the Fundamental Research Foundation of Tsinghua University (grant no. JZ2000007).

Appendix A

The functions $\lambda_j^{(\alpha)}(s,p)$ $(j=1,\ldots,6)$ in Eqs. (7) are the roots of the following equation

$$\mathrm{Det}[\mathbf{D}(s,p,\lambda)]=0, \tag{A.1}$$

where the matrix $\mathbf{D}(s,p,\lambda)$ is given by

$$\mathbf{D}(s,p,\lambda)=\begin{bmatrix} c_{44}\lambda^2-c_{11}s^2-\rho p^2 & (c_{13}+c_{44})\lambda(-\mathrm{i}s) & (e_{13}+e_{15})\lambda(-\mathrm{i}s) \\ (c_{13}+c_{44})\lambda(-\mathrm{i}s) & c_{33}\lambda^2-c_{44}s^2-\rho p^2 & e_{33}\lambda^2-e_{15}s^2 \\ (e_{13}+e_{15})\lambda(-\mathrm{i}s) & e_{33}\lambda^2-e_{15}s^2 & -\varepsilon_{33}\lambda^2+\varepsilon_{11}s^2 \end{bmatrix}. \tag{A.2}$$

Then, the functions $a_j^{(\alpha)}(s,p), b_j^{(\alpha)}(s,p)$ $(j=1,\ldots,6)$ in Eq. (7) can be obtained by

$$a_j=\frac{\begin{vmatrix} -d_{11}(s,p,\lambda_j) & d_{13}(s,p,\lambda_j) \\ -d_{21}(s,p,\lambda_j) & d_{23}(s,p,\lambda_j) \end{vmatrix}}{\begin{vmatrix} d_{12}(s,p,\lambda_j) & d_{13}(s,p,\lambda_j) \\ d_{22}(s,p,\lambda_j) & d_{23}(s,p,\lambda_j) \end{vmatrix}}, \qquad b_j=\frac{\begin{vmatrix} d_{12}(s,p,\lambda_j) & -d_{11}(s,p,\lambda_j) \\ d_{22}(s,p,\lambda_j) & -d_{21}(s,p,\lambda_j) \end{vmatrix}}{\begin{vmatrix} d_{12}(s,p,\lambda_j) & d_{13}(s,p,\lambda_j) \\ d_{22}(s,p,\lambda_j) & d_{23}(s,p,\lambda_j) \end{vmatrix}}, \tag{A.3}$$

where $d_{mn}(s,p,\lambda)$ ($m=1,2$, and $n=1,2,3$) are the components of matrix $\mathbf{D}(s,p,\lambda)$.

Appendix B

The constant matrixes $\mathbf{A}$ and $\mathbf{B}$ in Eq. (9) can be expressed as

$$\mathbf{A}=\begin{bmatrix} 0 & M_{12} \\ M_{21} & 0 \end{bmatrix}, \qquad \mathbf{B}=\begin{bmatrix} M_{11} & 0 \\ 0 & M_{22} \end{bmatrix}, \tag{B.1}$$

where

$$
\begin{aligned}
&M_{ij} = \lim_{s\to\infty}[K_{ij}(s,p)], \quad (i,j=1,2)\\
&K_{11} = \mathrm{i}\sum_{j=1}^{6}\frac{h_{8j}\Delta_{10j}}{(-\mathrm{i}s)\Delta}, \qquad K_{12} = \sum_{j=1}^{6}\frac{h_{8j}\Delta_{11j}}{(-\mathrm{i}s)\Delta},\\
&K_{21} = \sum_{j=1}^{6}\frac{h_{7j}\Delta_{10j}}{(-\mathrm{i}s)\Delta}, \qquad K_{22} = \mathrm{i}\sum_{j=1}^{6}\frac{h_{7j}\Delta_{11j}}{(-\mathrm{i}s)\Delta},
\end{aligned}
\tag{B.2}
$$

with $\Delta = \mathrm{Det}(\mathbf{H})$ and the $\mathbf{H}$ matrix being given below. h_{kj} is the component of $\mathbf{H}$ of the kth line and the jth row. Δ_{kj} is the algebraic complements corresponding to h_{kj}. The components of $\mathbf{H}$ are given by

$$
\begin{aligned}
&h_{1j} = \left[c_{13}^{(1)}(-\mathrm{i}s) + c_{33}^{(1)}a_j^{(1)}\lambda_j^{(1)} + e_{33}^{(1)}b_j^{(1)}\lambda_j^{(1)}\right]\mathrm{e}^{\lambda_j^{(1)}h_1}, \qquad h_{1(j+6)} = 0,\\
&h_{2j} = \left[c_{44}^{(1)}\lambda_j^{(1)} + c_{44}^{(1)}a_j^{(1)}(-\mathrm{i}s) + e_{15}^{(1)}b_j^{(1)}(-\mathrm{i}s)\right]\mathrm{e}^{\lambda_j^{(1)}h_1}, \qquad h_{2(j+6)} = 0,\\
&h_{3j} = \left[e_{13}^{(1)}(-\mathrm{i}s) + e_{33}^{(1)}a_j^{(1)}\lambda_j^{(1)} - \varepsilon_{33}^{(1)}b_j^{(1)}\lambda_j^{(1)}\right]\mathrm{e}^{\lambda_j^{(1)}h_1}, \qquad h_{3(j+6)} = 0,\\
&h_{4j} = 0, \qquad h_{4(j+6)} = \left[c_{13}^{(2)}(-\mathrm{i}s) + c_{33}^{(2)}a_j^{(2)}\lambda_j^{(2)} + e_{33}^{(2)}b_j^{(2)}\lambda_j^{(2)}\right]\mathrm{e}^{-\lambda_j^{(2)}h_2},\\
&h_{5j} = 0, \qquad h_{5(j+6)} = \left[c_{44}^{(2)}\lambda_j^{(2)} + c_{44}^{(2)}a_j^{(2)}(-\mathrm{i}s) + e_{15}^{(2)}b_j^{(2)}(-\mathrm{i}s)\right]\mathrm{e}^{-\lambda_j^{(2)}h_2},\\
&h_{6j} = 0, \qquad h_{6(j+6)} = \left[e_{13}^{(2)}(-\mathrm{i}s) + e_{33}^{(2)}a_j^{(2)}\lambda_j^{(2)} - \varepsilon_{33}^{(2)}b_j^{(2)}\lambda_j^{(2)}\right]\mathrm{e}^{-\lambda_j^{(2)}h_2},\\
&h_{7j} = \left[c_{13}^{(1)}(-\mathrm{i}s) + c_{33}^{(1)}a_j^{(1)}\lambda_j^{(1)} + e_{33}^{(1)}b_j^{(1)}\lambda_j^{(1)}\right],\\
&h_{7(j+6)} = -\left[c_{13}^{(2)}(-\mathrm{i}s) + c_{33}^{(2)}a_j^{(2)}\lambda_j^{(2)} + e_{33}^{(2)}b_j^{(2)}\lambda_j^{(2)}\right],\\
&h_{8j} = \left[c_{44}^{(1)}\lambda_j^{(1)} + c_{44}^{(1)}a_j^{(1)}(-\mathrm{i}s) + e_{15}^{(1)}b_j^{(1)}(-\mathrm{i}s)\right],\\
&h_{8(j+6)} = -\left[c_{44}^{(2)}\lambda_j^{(2)} + c_{44}^{(2)}a_j^{(2)}(-\mathrm{i}s) + e_{15}^{(2)}b_j^{(2)}(-\mathrm{i}s)\right],\\
&h_{9j} = \left[e_{13}^{(1)}(-\mathrm{i}s) + e_{33}^{(1)}a_j^{(1)}\lambda_j^{(1)} - \varepsilon_{33}^{(1)}b_j^{(1)}\lambda_j^{(1)}\right],\\
&h_{9(j+6)} = -\left[e_{13}^{(2)}(-\mathrm{i}s) + e_{33}^{(2)}a_j^{(2)}\lambda_j^{(2)} - \varepsilon_{33}^{(2)}b_j^{(2)}\lambda_j^{(2)}\right],\\
&h_{10j} = 1, \qquad h_{10(j+6)} = -1,\\
&h_{11j} = a_j^{(1)}, \qquad h_{11(j+6)} = -a_j^{(2)},\\
&h_{12j} = b_j^{(1)}, \qquad h_{12(j+6)} = -b_j^{(2)}, \quad (j=1,2,\ldots,6).
\end{aligned}
\tag{B.3}
$$

Then the functions matrix $\mathbf{Q}(x,t)$ in Eq. (9) can be written as

$$
\mathbf{Q}(x,t) = \begin{bmatrix} q_{11}(x,t) & q_{12}(x,t)\\ q_{21}(x,t) & q_{22}(x,t)\end{bmatrix}
\tag{B.4}
$$

with

$$
\begin{aligned}
&q_{11}(x,t) = \int_0^\infty [K_{11}(s,p) - M_{11}]\sin[s(t-x)]\,\mathrm{d}s,\\
&q_{12}(x,t) = \int_0^\infty [K_{12}(s,p) - M_{12}]\cos[s(t-x)]\,\mathrm{d}s,
\end{aligned}
$$

$$q_{21}(x,t) = \int_0^\infty [K_{21}(s,p) - M_{21}]\cos[s(t-x)]\,\mathrm{d}s,$$
$$q_{22}(x,t) = \int_0^\infty [K_{22}(s,p) - M_{22}]\sin[s(t-x)]\,\mathrm{d}s. \tag{B.5}$$

References

Chen, Z.T., Karihaloo, B.L., 1999. Dynamic response of a cracked piezoelectric ceramic under arbitrary electro-mechanical impact. Int. J. Solids Struct. 36, 5125–5133.

Chen, Z.T., Karihaloo, B.L., Yu, S.W., 1998. A Griffith crack moving along the interface of two dissimilar piezoelectric materials. Int. J. Fract. 91, 197–203.

Chen, Z.T., Yu, S.W., 1997. Antiplane dynamic fracture mechanics of piezoelectric materials. Int. J. Fract. 85, L3–L12.

Chen, Z.T., Yu, S.W., 1998. Semi-infinite crack under anti-plane mechanical impact in piezoelectric materials. Int. J. Fract. 88, L53–L56.

Gao, H., Zhang, T., Tong, P., 1997. Local and global energy rates for an electrically yielded crack in piezoelectric ceramics. J. Mech. Phys. Solids 45, 491–510.

Li, S.F., Mataga, P.A., 1996a. Dynamic crack propagation in piezoelectric materials—Part I: Electrode solution. J. Mech. Phys. Solids 44, 1799–1830.

Li, S.F., Mataga, P.A., 1996b. Dynamic crack propagation in piezoelectric materials—Part II: Vacuum solution. J. Mech. Phys. Solids 44, 1831–1866.

Narita, F., Shindo, Y., 1998. Scattering of Love waves by a surface-breaking crack in a piezoelectric layered medium. JSME Int. J. 41, 40–48.

Pak, Y., 1990. Crack extension force in a piezoelectric material. J. Appl. Mech. 57, 647–653.

Qin, Q.H., 2000. Fracture Mechanics of Piezoelectric Materials. WIT Press, Southampton.

Qin, Q.H., Zhang, X., 2000. Crack deflection at an interface between dissimilar piezoelectric materials. Int. J. Fract. 102, 355–370.

Shen, S.P., Kuang, Z.B., 1998. Wave scattering from an interface crack in laminated anisotropic media. Mech. Res. Comm. 25 (5), 509–517.

Shindo, Y., Katsura, H., Yan, W., 1996. Dynamic stress intensity factor of a cracked electric medium in an uniform electric field. Acta Mech. 117, 1–10.

Suo, Z., Kuo, C.M., Barnett, D.M., Willis, J.R., 1992. Fracture mechanics for piezoelectric ceramics. J. Mech. Phys. Solids 40 (4), 739–765.

Wang, T.C., Han, X.L., 1999. Fracture mechanics of piezoelectric materials. Int. J. Fract. 98, 15–35.

Wang, X.Y., Yu, S.W., 2000. Transient response of a Crack in piezoelectric strip subjected to mechanical and electrical impacts: mode-I problem. Mech. Mater. 33 (1), 11–20.